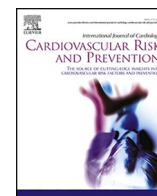




Contents lists available at ScienceDirect

International Journal of Cardiology Cardiovascular Risk and Prevention

journal homepage: www.journals.elsevier.com/international-journal-of-cardiology-cardiovascular-risk-and-prevention



Associations between urinary and blood heavy metal exposure and heart failure in elderly adults: Insights from an interpretable machine learning model based on NHANES (2003–2020)[☆]

Yang Yuting^{a,b}, Deng Shan^{a,b,c,d,*}

^a Department of Cardiology, Union Hospital, Tongji Medical College, Huazhong University of Science and Technology, Wuhan 430022, China

^b Clinic Center of Human Gene Research, Union Hospital, Tongji Medical College, Huazhong University of Science and Technology, 1277 Jiefang Ave, Wuhan, 430022, China

^c Hubei Key Laboratory of Metabolic Abnormalities and Vascular Aging, Huazhong University of Science and Technology, Wuhan, China

^d Hubei Clinical Research Center for Metabolic and Cardiovascular Disease, Huazhong University of Science and Technology, Wuhan, China

ARTICLE INFO

Handling editor: D Levy

ABSTRACT

Background: The relationship between heavy metal exposure and heart failure is complex and poorly understood. This study employs machine learning techniques to model these associations in a population aged 50 years and older from the National Health and Nutrition Examination Survey (NHANES). Our findings emphasize the need for continued investigation into the mechanisms of these associations and highlight the importance of monitoring and regulatory measures to mitigate heavy metal exposure in populations at risk.

Methods: Five machine learning models were evaluated, with Gradient Boosting Decision Trees (GBDT) selected as the optimal model based on accuracy, interpretability, and ability to capture nonlinear relationships. Model performance was assessed through various metrics, and interpretability was enhanced using SHAP (SHapley Additive exPlanations), permuted Feature Importance, Individual Conditional Expectation (ICE), and Partial Dependence Plots (PDP).

Results: The GBDT model achieved an accuracy of 0.78, with a sensitivity of 0.93 and an AUC of 0.92. Our analysis revealed that higher levels of urinary iodine, blood cadmium, urinary cobalt, urinary tungsten, and urinary arsenic acid were significantly associated with heart failure. Synergistic effects involving age and body mass index (BMI) were also observed, further strengthening these associations.

1. Introduction

Individuals are unavoidably exposed to environments containing heavy metals, and these elements can infiltrate the human body via ingestion and inhalation [1]. The threat of heavy metals to human health continues to exist and has now become a global public health issue. Heavy metals typically function by displacing essential metal ions in the human body [2], leading to disruptions in critical biological pathways. Such disruptions can result in endothelial cell damage [3–5], disturbances in lipid metabolism [6], increased oxidative stress [7,8], immune homeostasis imbalance [9,10], and epigenetic modifications [11], all of which may contribute to the development of various

cardiovascular diseases. Exposure to heavy metals during pregnancy has been linked to an increased risk of congenital heart defects in offspring [12,13]. Additionally, exposure in preschool children may lead to arrhythmias [14], while heavy metal exposure has been associated with hypertension [15]. The impact of exposure to some heavy metals on the incidence of heart failure has also been studied [16,17].

Heart failure isn't a standalone illness but rather the end stage of various heart diseases, which continues to be a significant contributor to mortality, morbidity, and diminished quality of life globally [18]. Heart failure impacts the health of more than 60 million people worldwide [19], and the lifetime risk of heart failure has risen to 24 %, roughly one in four people will develop heart failure in their lifetime [20]. Research

[☆] Although the manuscript will be submitted and handled by the corresponding author (Deng Shan), the primary point of contact for the editorial and review process will be the first author (Yang Yuting), who will be responsible for answering any queries regarding the manuscript during peer review, revision, and final publication.

* Corresponding author. Department of Cardiology, Union Hospital, Tongji Medical College, Huazhong University of Science and Technology, Wuhan, China.

E-mail addresses: m202275882@hust.edu.cn (Y. Yuting), dengshan1020@hust.edu.cn (D. Shan).

<https://doi.org/10.1016/j.ijcrp.2025.200418>

Received 30 January 2025; Received in revised form 4 April 2025; Accepted 30 April 2025

Available online 4 May 2025

2772-4875/© 2025 The Authors. Published by Elsevier B.V. This is an open access article under the CC BY-NC-ND license (<http://creativecommons.org/licenses/by-nc-nd/4.0/>).

indicates a significant correlation between cadmium exposure and the incidence of heart failure [21–24]. And the level of urinary antimony appears to be directly proportional to the risk of heart failure [25]. Besides, epidemiological research has indicated that exposure to cobalt and lead elevates the risk of heart failure [16,26]. However, previous research has predominantly relied on conventional statistical methods, which exhibit limited flexibility in modeling complex relationships and often operate under restrictive assumptions regarding underlying data distributions [27]. Furthermore, much of the existing literature has focused on examining the effects of a single type of heavy metal in isolation. This approach may overlook potential interactions and cumulative effects of multiple heavy metals, thereby limiting the comprehensiveness of the findings. Thus, a more integrated and flexible modeling framework, machine learning, may be necessary to capture the intricacies of heavy metal exposure and its multifaceted impact on heart failure.

Our study conducted a comprehensive analysis of laboratory indicators for various heavy metal elements in both blood and urine, utilizing data from the National Health and Nutrition Examination Survey (NHANES) database spanning 2003 to 2020. This robust database provides high-quality, nationally representative data essential for public health research, integrating interviews, physical examinations, and laboratory assessments. Furthermore, we employed advanced machine learning algorithms for the analysis, enhancing our ability to uncover meaningful relationships within the data. Machine learning tends to prioritize predictive performance and generalization over interpretability, with a mathematical emphasis on cross-validation and iterative enhancement of algorithms [28]. This implies that machine learning algorithms frequently outshine traditional statistical prediction methods, however, less transparent compared to conventional statistical approaches. Consequently, there is a need for explanatory models in machine learning. SHAP (SHapley Additive exPlanations) is a technique for interpreting machine learning models, employing the computation of Shapley values to ascertain the contribution of each feature to a given prediction, and thus facilitates the generation of transparent explanations by leveraging these calculated Shapley values [29,30]. In this study, we chose five machine learning algorithms for our analysis, identified the best-performing model, and utilized the SHAP model for interpreting.

2. Methods

2.1. Data source

All variable information was sourced from the NHANES (the National Health and Nutrition Examination Survey) database (<http://www.cdc.gov/Nchs/Nhanes>). The NHANES database, carried out by the Centers for Disease Control and Prevention (CDC) in the United States, combines interviews, laboratory tests and physical examinations on a nationally representative sample of American residents every two years. We downloaded the variables data from the annual datasets of NHANES 2003–2004, NHANES 2005–2006, NHANES 2007–2008, NHANES 2009–2010, NHANES 2011–2012, NHANES 2013–2014, NHANES 2015–2016, NHANES 2017–2018, and NHANES 2019–2020, match all variables for each year by the unique sequence numbers, and ultimately merged the datasets for all the years. The features and labels encompassed in the study include gender, age (year), race, education level, poverty-to-income ratio (PIR), height, weight, body mass index (BMI, kg/m^2), urinary heavy metals (including urine mercury, urine barium, urine beryllium, urine cadmium, urine cobalt, urine cesium, urine molybdenum, urine lead, urine platinum, urine antimony, urine thallium, urine tungsten, urine uranium, urine arsenous acid, urine arsenobetaine, urine arsenocholine, urine dimethylarsonic acid, urine monomethylarsonic acid, urine total arsenic, and urine iodine), blood heavy metals (including blood cadmium, blood lead, blood mercury), and heart failure. The diagnosis of heart failure is

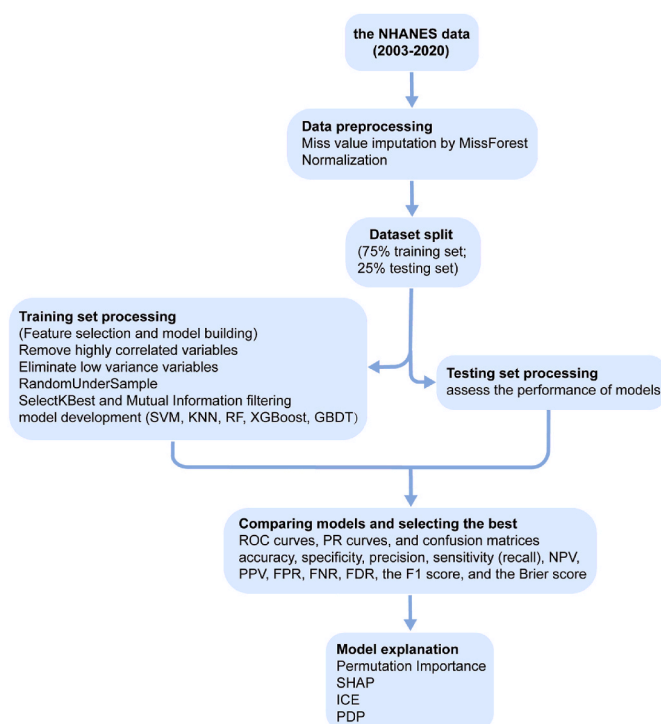


Fig. 1. Machine learning model development flowchart. This flowchart outlines the key steps in developing a machine learning model from inception to interpretation.

ascertained through self-reported physician diagnoses acquired via standardized medical questionnaires in individual interviews. Participants were queried: "Has a doctor or other health professional ever told that you had congestive heart failure?" If a person responds 'yes', they will be regarded as having heart failure. According to the 10th revised edition of the International Classification of Diseases and Related Health Problems (ICD-10), the code for congestive heart failure is I50.0, I50.1, I50.9 [31]. Heavy metal samples in blood and urine were processed, stored, and transported to the Centers for Disease Control and Prevention and the Science Department of the Environmental Health Laboratory of the National Environmental Health Center for analysis.

2.2. Study population

The inclusion criteria were as follows: (1) participants were aged 50 or above; (2) participants underwent heavy metal laboratory testing in blood and urine samples; (3) heart failure status was 1 (ever had a heart failure) or 2 (didn't have a heart failure) based on the NHANES questionnaires. Exclusion criteria were as follows: (1) heart failure status was 7 (refused to answer this question) or 9 (means uncertain heart failure status) according to NHANES questionnaires. Finally, a total of 6879 participants were included in the present analysis.

2.3. Statistical analysis

2.3.1. Statistical description of baseline characteristics between heart failure group and no heart failure group

The demographic description section was analyzed using R 4.2.3. In the baseline table, we divided the participants into the heart failure group and the no heart failure group for comparison. The baseline covariates were presented as mean (standard deviation) for continuous variables and count (percentage) for categorical variables, respectively. The t tests and χ^2 tests were employed to compare the differences between the groups for continuous and categorical variables, separately. variables associated with heavy metals concentration were depicted

using geometric mean and geometric standard deviation.

2.3.2. Machine learning processing

2.3.2.1. *Data preprocessing and splitting.* The analysis of the machine learning section is accomplished using Python 3.10.8 and Python libraries, including “sklearn”, “imblearn”, “numpy”, and “pandas”. An overview of our methodology is presented in (Fig. 1). BMI, age, gender, blood heavy metals, and urinary heavy metals were selected as feature variables, and heart failure as the target variable for the machine learning model. “missForest” was used for missing value imputation, which is an iterative imputation approach based on random forest method and can concurrently interpolate different types of data [32]. The raw data was standardized using the “StandardScaler” function. The dataset was randomly split into a training set (N = 5159) and a testing set (N = 1720) in accordance with a specific ratio, with the training set constituting 75 % of all the dataset. We calculated the Pearson correlation coefficients of all predictor variable in the training set and plotted heatmaps respectively before and after deleting highly correlated variables (Supplementary Fig. 1). To reduce the influence of multicollinearity on the model, features with Pearson coefficients exceeding 0.8 were removed [33]. The low variance features have been removed, which possess limited explanatory information and make a minor contribution to the model’s predictive capacity.

2.3.2.2. *Feature selection and model training.* After the initial feature filtering via the above-mentioned steps, we incorporated a pipeline consisting of “RandomUnderSample”, “SelectKBest”, and the model classifier for the subsequent analysis. Among the pipeline process, RUS (RandomUnderSample) is a sampling method that can create balanced classes from imbalanced ones [34,35], and “SelectKBest” is a feature selection method that functions by scoring all features and selecting the top “k” input variables with the highest scores [36] (mutual information was selected as the scoring metric, with higher scores indicating a stronger correlation between the variables [37]). Grid search was used for hyperparameter tuning, thereby selecting the optimal hyperparameter values for each machine learning model [38] (The detailed parameter information for the model is provided in the supplementary materials). We chose five machine learning models: SVM (Support Vector Machine), RF (Random Forest), XGBoost (eXtreme Gradient Boosting), GDBT (Gradient Boosting Decision Tree), and KNN (k-nearest neighbor). Among them, the GDBT was found to be the best one.

2.3.2.3. *Model evaluation and comparison.* To conduct a thorough and systematic comparison of the machine learning models, we employed a multifaceted approach that included generating various evaluation plots alongside calculating a comprehensive set of performance metrics both in the training and testing sets. Specifically, we constructed Receiver Operating Characteristic (ROC) curves, precision-recall (PR) curves, and confusion matrices. The ROC curves provide insight into the model’s diagnostic capabilities and the PR curves offer a focused analysis of the model’s performance in classifying positive cases, particularly in imbalanced datasets. Confusion matrices were used to provide a detailed breakdown of the models’ classification results, highlighting the number of true positives, true negatives, false positives, and false negatives. We further calculated a comprehensive suite of quantitative metrics, including accuracy, specificity, precision, sensitivity (recall), negative predictive value (NPV), positive predictive value (PPV), false positive rate (FPR), false negative rate (FNR), false discovery rate (FDR), the F1 score, and the Brier score. These metrics collectively elucidated the models’ classification efficacy, with the F1 score serving to balance precision and recall and the Brier score reflecting the probabilistic accuracy of predictions. Moreover, we evaluated the area under the ROC curve (AUC) and its 95 % confidence intervals as a measure of the models’ overall ability to distinguish between positive and negative

Table 1

Baseline characteristics of study participants. All continuous demographic variables are presented as mean (standard deviation), while the categorical variables are presented as frequency (percentage). Variables related to heavy metals are represented using geometric mean (geometric standard deviation). Statistical comparisons between the heart failure and no heart failure groups were conducted using Student’s t-test for continuous variables and chi-square tests for categorical variables, with a significance level set at $p < 0.05$. BMI: Body Mass Index is calculated as weight in kilograms divided by the square of height in meters; PIR: Poverty to Income Ratio is calculated based on household income relative to the federal poverty line.

Characteristics	Total adults (N = 6879)	Heart failure (N = 388)	No heart failure (N = 6491)	P value
Age, years, mean (SD)	65.58(9.06)	69.74(8.39)	65.33(9.04)	<0.01
Gender, n (%)				<0.01
Male	3454(50.2)	233(60.1)	3221(49.6)	
Female	3425(49.8)	155(39.9)	3270(50.4)	
BMI, kg/m ² , mean (SD)	29.72(8.07)	32.92(16.51)	29.53(7.22)	<0.01
Weight status, n (%)				<0.01
BMI <25	1727(25.1)	79(20.4)	1648(25.4)	
BMI ≥ 25 & <30	2391(34.8)	108(27.8)	2283(35.2)	
BMI ≥ 30	2761(40.1)	201(51.8)	2560(39.4)	
Race, n(%)				<0.01
Mexican American	812(11.8)	27(7)	785(12.1)	
Hispanic	714(10.4)	31(8)	683(10.5)	
Non-Hispanic White	2954(42.9)	196(50.5)	2758(42.5)	
Non-Hispanic Black	1613(23.4)	109(28.1)	1504(23.2)	
Other Race (Including Multi- Racial)	786(11.4)	25(6.4)	761(11.7)	
Education, n (%)				<0.01
Grades 0-12	1900(27.6)	118(30.4)	1782(27.5)	
High school graduate/GED or equivalent	3485(50.7)	223(57.5)	3262(50.3)	
College graduate or above	1494(21.7)	47(12.1)	1447(22.3)	
PIR, mean (SE)	2.61(1.56)	2.02(1.31)	2.65(1.56)	<0.01
PIR level, n (%)				<0.01
Low (<1)	1112(16.2)	83(21.4)	1029(15.9)	
Medium (≥1 & <4)	4061(59)	257(66.2)	3804(58.6)	
High (≥4)	1706(24.8)	48(12.4)	1658(25.5)	
Blood heavy metals, geometric mean (GSD)				
Cadmium (µg/L)	0.40(0.76)	0.48(0.79)	0.40(0.76)	<0.01
Lead (µg/dL)	1.47(0.62)	1.63(0.61)	1.46(0.62)	0.02
Mercury, total (µg/L)	0.95(1.01)	0.72(0.89)	0.96(1.02)	<0.01
Urinary heavy metals, geometric mean (GSD)				
Mercury (µg/L)	0.30(1.08)	0.25(1.05)	0.30(1.08)	0.05
Barium (µg/L)	0.96(1.03)	0.83(1.09)	0.97(1.02)	0.55
Beryllium (µg/L)	0.60(1.50)	0.55(1.41)	0.60(1.50)	<0.01
Cadmium (µg/L)	0.32(0.98)	0.37(0.98)	0.31(0.98)	<0.01
Cobalt (µg/L)	0.34(0.88)	0.43(0.91)	0.34(0.87)	0.15
Cesium (µg/L)	4.09(0.65)	3.63(0.60)	4.12(0.65)	<0.01
Molybdenum (µg/L)	34.86(0.87)	36.14(0.79)	34.79(0.70)	0.83
Lead (µg/L)	0.48(0.89)	0.49(0.94)	0.48(0.89)	0.49
Platinum (µg/L)	0.40(2.47)	0.38(2.38)	0.40(2.48)	0.08
Antimony (µg/L)	0.05(0.98)	0.07(1.22)	0.05(0.97)	<0.01
Thallium (µg/L)	0.15(0.81)	0.15(0.10)	0.15(0.80)	<0.01
Tungsten (µg/L)	0.06(1.14)	0.09(1.26)	0.06(1.13)	<0.01
Uranium (µg/L)	0.03(2.11)	0.04(2.31)	0.03(2.10)	<0.01
Arsenous acid (µg/L)	0.30(1.12)	0.30(1.16)	0.30(1.12)	0.1
Arsenic acid (µg/L)	0.64(0.24)	0.66(0.31)	0.63(0.24)	0.23
Arsenobetaine (µg/L)	2.51(1.54)	2.50(1.47)	2.51(1.54)	0.14
Arsenocholine (µg/L)	0.18(0.91)	0.20(0.99)	0.18(0.90)	0.21
Dimethylarsonic acid (µg/L)	3.63(0.81)	3.23(0.71)	3.66(0.82)	<0.01
Monomethylarsonic acid (µg/L)	0.48(0.91)	0.50(0.89)	0.47(0.91)	0.86
Total arsenic (µg/L)	8.55(1.16)	7.80(1.06)	8.60(1.17)	0.03
Iodine (ng/mL)	146.76(0.95)	183.23(1.28)	144.83(0.92)	<0.01

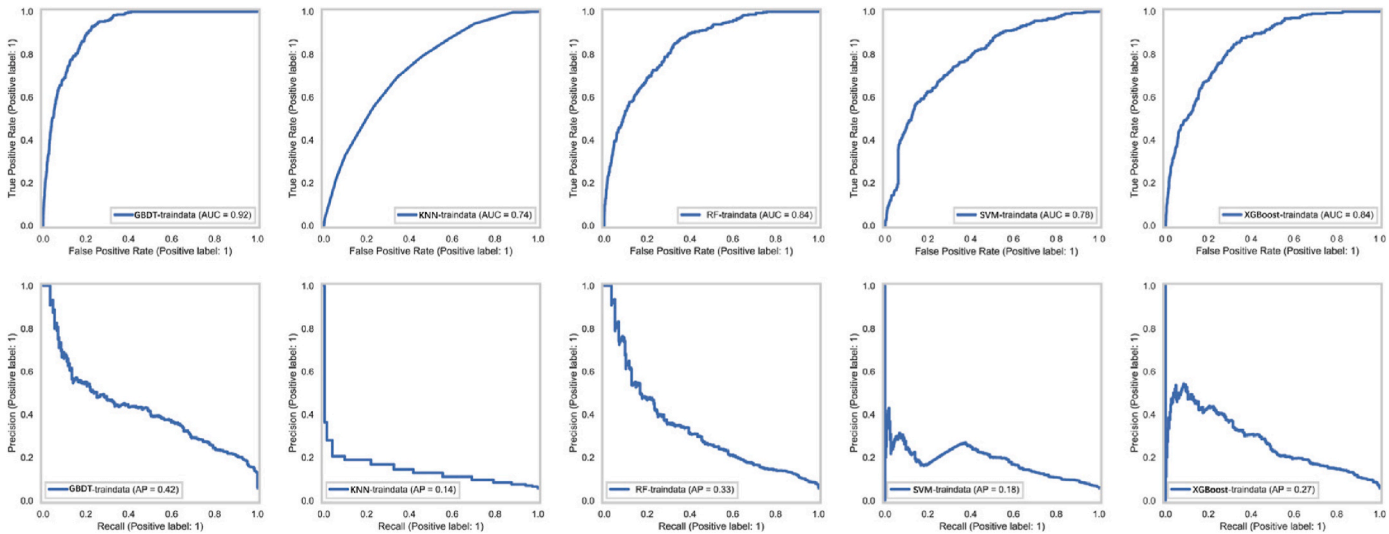


Fig. 2. ROC and PR curves of the five models in the training set. The figure depicts the ROC curves and PR curves for 5 predictive models: GBDT, KNN, RF, SVM, and XGBoost. Each model’s performance is shown, demonstrating its ability to distinguish between the positive and negative classes (ROC) and the balance between precision and recall (PR).

classes, complemented by the average precision score (AP) to quantify performance in scenarios characterized by class imbalance.

2.3.2.4. Model explanation. In the explanation section of the optimal model, we calculated the PI (permutation importance) values of each feature in the model, constructed the SHAP (SHapley Additive exPlanations) explanation model using the “shap” package [39], and plotted ICE (Individual Conditional Expectation) plot and PDP (Partial Dependence Plot) to respectively demonstrate the impact of a single feature and two features on the target.

3. Results

3.1. Baseline characteristics

Among 6879 participants, 388 were diagnosed with heart failure, while 6491 were classified as having no heart failure. As illustrated in Table 1, a substantial proportion of the baseline characteristics exhibited significant statistical differences between the heart failure group and the group without heart failure. Compared to participants without heart failure, those in the heart failure group exhibited a higher age ($69.74 \pm$

8.39 versus 65.33 ± 9.04 ; $P < 0.01$), a greater proportion of male participants (60.1% versus 49.6% ; $P < 0.01$), and an elevated BMI (32.92 ± 16.51 versus 29.53 ± 7.22 ; $P < 0.01$). Besides, significant statistical differences (P Value < 0.05) were observed in the laboratory indicators of heavy metals, including blood cadmium, blood lead, blood mercury, urinary beryllium, urinary cadmium, urinary cesium, urinary antimony, urinary thallium, urinary tungsten, urinary uranium, urinary dimethylarsonic acid, urinary total arsenic, and urinary iodine, between the two participant groups.

3.2. Comparison of machine learning models

Considering our dataset is imbalanced, performance metrics that account for class distribution, such as sensitivity (recall), precision, F1 score, and AUC, become more crucial in determining which model is the best, compared with other evaluating indicators. Fig. 2 illustrates the ROC curves and PR curves for the five machine learning models for the training set, presented separately. The AUC for GBDT was 0.92 (95 % CI: 0.91–0.93), indicating superior predictive performance in distinguishing heart failure compared to the four other models. The RF yielded an AUC of 0.84 (95 % CI: 0.82–0.86), which was similar to that of XGBoost,

Table 2
Evaluation indicators for predictive models. NPV: Negative Predictive Value. FPR: False Positive Rate. FNR: False Negative Rate. FDR: False Discovery Rate. F1 score: The harmonic mean of precision and recall, calculated as $2 * (\text{Precision} * \text{Recall}) / (\text{Precision} + \text{Recall})$. AUC: Area Under the Curve. AP: Average Precision.

Model	GBDT	GBDT	KNN	KNN	RF	RF	SVM	SVM	XGBoost	XGBoost
Dataset	Training	Testing	Training	Testing	Training	Testing	Training	Testing	Training	Testing
Accuracy	0.78	0.75	0.76	0.74	0.68	0.67	0.8	0.77	0.69	0.68
Sensitivity	0.93	0.71	0.56	0.57	0.85	0.7	0.62	0.58	0.84	0.65
Specificity	0.77	0.75	0.77	0.75	0.67	0.67	0.81	0.78	0.68	0.68
Precision	0.2	0.14	0.13	0.11	0.14	0.1	0.16	0.13	0.14	0.1
Recall	0.93	0.71	0.56	0.57	0.85	0.7	0.62	0.58	0.84	0.65
NPV	0.99	0.98	0.97	0.97	0.99	0.98	0.97	0.97	0.99	0.97
PPV	0.2	0.14	0.13	0.11	0.14	0.1	0.16	0.13	0.14	0.1
FPR	0.23	0.25	0.23	0.25	0.33	0.33	0.19	0.22	0.32	0.32
FNR	0.07	0.29	0.44	0.43	0.15	0.3	0.38	0.42	0.16	0.35
FDR	0.8	0.86	0.87	0.89	0.86	0.9	0.84	0.87	0.86	0.9
F1 score	0.33	0.23	0.21	0.19	0.24	0.18	0.26	0.21	0.24	0.17
Brier score	0.18	0.19	0.21	0.22	0.2	0.21	0.21	0.22	0.21	0.21
AUC	0.92	0.81	0.74	0.73	0.84	0.77	0.78	0.75	0.84	0.75
AUC_low	0.91	0.77	0.71	0.68	0.82	0.73	0.76	0.69	0.82	0.7
AUC_up	0.93	0.85	0.76	0.78	0.86	0.82	0.81	0.8	0.86	0.8
AP score	0.42	0.17	0.14	0.11	0.33	0.14	0.18	0.12	0.27	0.15

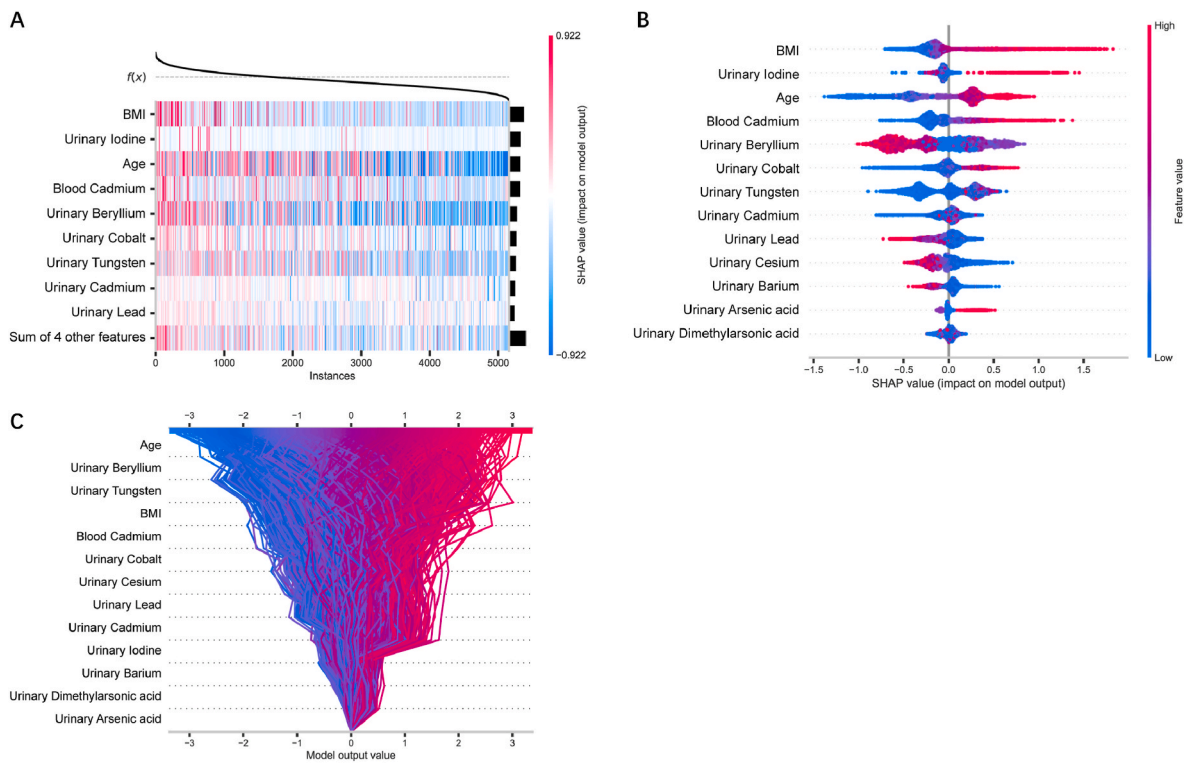


Fig. 3. SHAP visualizations for model interpretation. **Fig. 3A:** SHAP heatmap. The y-axis displays different features arranged in descending order based on their maximum absolute SHAP values, indicating their relative contributions to the prediction of heart failure outcomes. The x-axis represents individual observations from the dataset. Each cell in the heatmap is color-coded to reflect the SHAP values, with red indicating positive contributions to heart failure and blue representing negative contributions. **Fig. 3B:** SHAP beeswarm map. The features on the y-axis are organized in the same order as those in the heatmap. The x-axis quantifies the SHAP values, reflecting the impact of each feature on the model's predictions. Each point on the plot corresponds to a specific observation, with colors representing feature value levels; red indicates higher levels while blue denotes lower levels. **Fig. 3C:** SHAP decision map. Illustrates individual predictions in relation to the cumulative effects of features, showing how each feature contributes to the final decision. Blue indicates negative predictions, while red indicates positive predictions. (For interpretation of the references to color in this figure legend, the reader is referred to the Web version of this article.)

at 0.84 (95 % CI: 0.82–0.86), suggesting robust performance. In contrast, the SVM achieved an AUC of 0.78 (95 % CI: 0.76–0.81), while the K-Nearest Neighbors (KNN) model had an AUC of 0.74 (95 % CI:

0.71–0.76), indicating a moderate discrimination ability. Besides, GBDT stand out with the highest average precision score, demonstrating superior capability in maintaining precision and better diagnostic

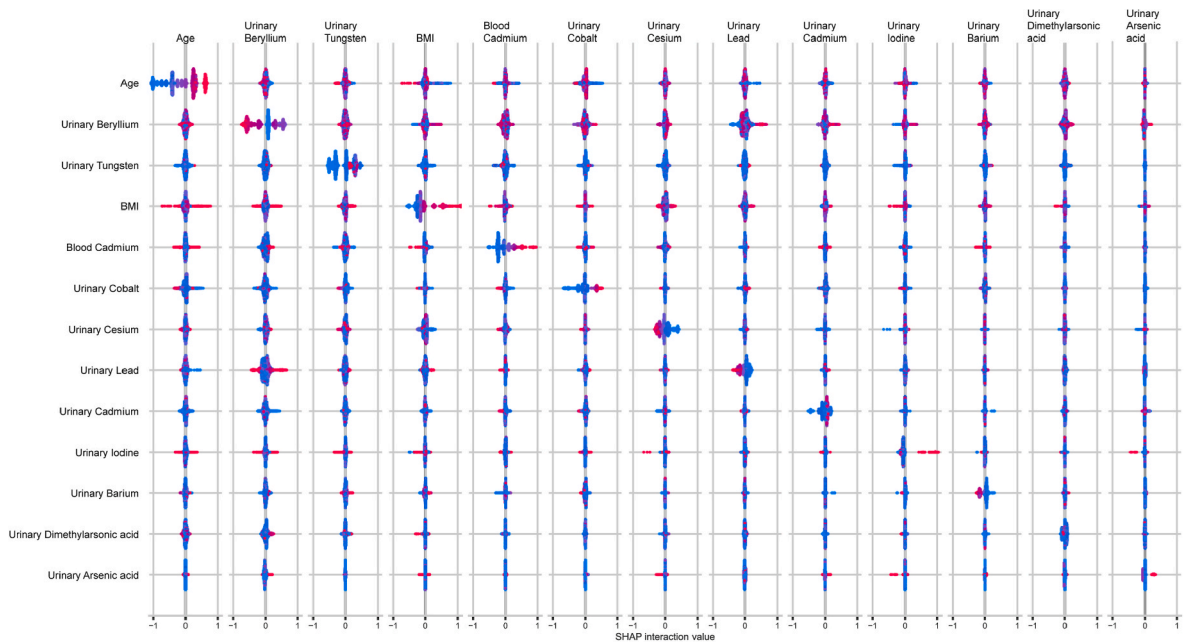


Fig. 4. SHAP interaction plot. Illustrate the combined effects of two features on model predictions.

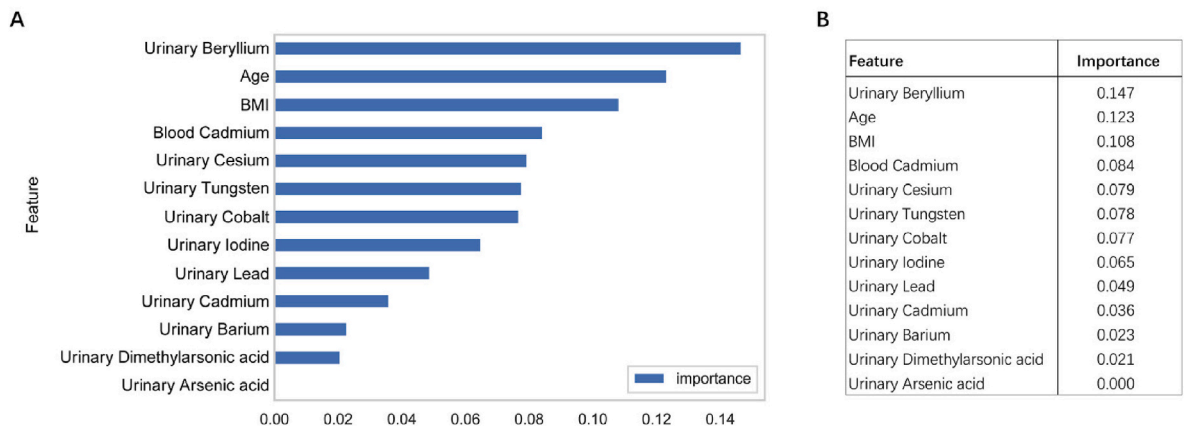


Fig. 5. Premutation importance analysis. The figure evaluates the contribution of individual features to the model’s predictive performance through permutation importance analysis. **Fig. 5A:** Bar plot of feature importance scores, ranking the features according to their significance. **Fig. 5B:** Table displaying the feature importance scores.

accuracy in heart failure compared to other models. Table 2 presents specific evaluation metrics for five machine learning models. GBDT achieves a sensitivity of 0.93, indicating excellent true positive identification. In contrast, KNN and SVM exhibit considerably lower sensitivities of 0.56 and 0.61, respectively, resulting in a greater likelihood of missing actual heart failure cases. Overall, GBDT demonstrates distinct advantages over KNN, RF, SVM, and XGBoost based on these performance metrics. Its superior sensitivity (0.93), Average Precision Score (APS) of 0.42, and accuracy of 0.78 position GBDT as an exceptional choice for predictive modeling in scenarios where both precision and recall are essential. The ROC curves and PR curves for the testing set are presented in Supplementary Fig. 2, and Supplementary Fig. 3 displays the corresponding confusion matrices.

3.3. The explainability of the best machine learning model

3.3.1. SHAP visualization plot

Fig. 3A presents a SHAP heatmap delineating the contributions of various features to the GBDT-derived predictions of heart failure, offering interpretable insights into the model’s decision-making process. The model’s output is shown above the heatmap, centered around the expected SHAP values for all observations. Additionally, the global importance of each input feature is depicted as a bar plot on the right side of the heatmap. Notably, BMI, urinary iodine, age, and blood cadmium emerge significant contributors to the model’s predictions. Fig. 3B presents the SHAP beeswarm plot for GBDT, illustrating the directional impact of each feature value on heart failure. Features such as urinary iodine, blood cadmium, urinary cobalt, body mass index (BMI), and age occupy the top positions and exhibit significant positive SHAP values, suggesting a strong positive association with heart failure classification. Urinary tungsten, urinary cadmium, and urinary arsenic acid are positioned further down the y-axis with lower SHAP value, indicating a modest positive contribution to heart failure classification. Interestingly, lower levels of urinary beryllium, urinary lead, urinary cesium, and urinary barium are associated with higher SHAP values, suggesting a potential protective effect against heart failure. The SHAP decision plot for GBDT is illustrated in Fig. 3C. Each line represents an individual participant, with the trajectory of each line converging from the bottom and extending toward the top indicating how the features influence the model’s output for specific instances. Fig. 4 depicts the SHAP interaction summary plot, where the horizontal axis represents interaction values that quantify the attribution of paired interaction effects between two features. Most variables demonstrate varying degrees of interaction effects. Features such as age, urinary beryllium, urinary tungsten, and BMI exhibit significant interaction effects with other variables, indicating the intricate multivariate relationships associated with heart failure.

3.3.2. Permutation importance analysis

The permutation importance analysis was conducted to estimate the contribution of features to the prediction of heart failure within GBDT by measuring the decrease in the model’s performance when the values of a feature were randomly shuffled (Fig. 5). The results revealed that urinary beryllium and blood cadmium exhibited the highest importance scores of 0.147 and 0.084 among the heavy metal variables, indicating their significant influence on predictive accuracy. Age and BMI were identified as important determinants, with scores of 0.123 and 0.108, respectively.

3.3.3. ICE plot and PDP plot

The ICE plots (Fig. 6), generated through partial conditional expectation, illustrated that the predicted probability of heart failure increases with rising levels of age, BMI, and blood cadmium, highlighting their potential relevance in heart failure classification. The relationship between urinary beryllium and heart failure was characterized by an inverted U-shaped curve, suggesting increased model sensitivity within a specific range of exposure. Other assessed features displayed moderate effects, indicating their contribution to prediction but with less pronounced impacts. Additionally, the two-dimensional PDP plot clarified the joint predictive effects of the top three heavy metal variables in the permutation importance analysis, alongside age and gender, on heart failure classification (Fig. 7). The color gradient, ranging from deep blue (higher predicted probability) to light green (lower), visualizes the interactions. Notably, blood cadmium interacted synergistically with age and gender, suggesting potential combined effects in shaping the model’s outputs.

4. Discussion

This study employed five machine learning models to explore the complex associations between heavy metal exposure in blood and urine and heart failure. Following a thorough evaluation of various model performance metrics, the GBDT model was chosen as the optimal predictive model due to its superior accuracy and interpretability. To further explain the findings derived from GBDT, several machine learning interpretability techniques were applied, including SHAP (SHapley Additive exPlanations), permuted Feature Importance, individual conditional expectation (ICE), and partial dependence plots (PDP). These methods enabled a comprehensive assessment of the individual contributions of each feature to heart failure, as well as interactions between pairs of features, offering valuable insights into the prediction on heart failure. Notably, the interplay between different heavy metals and other demographic factors, including age and BMI, suggests that risk assessments for heart failure must consider these

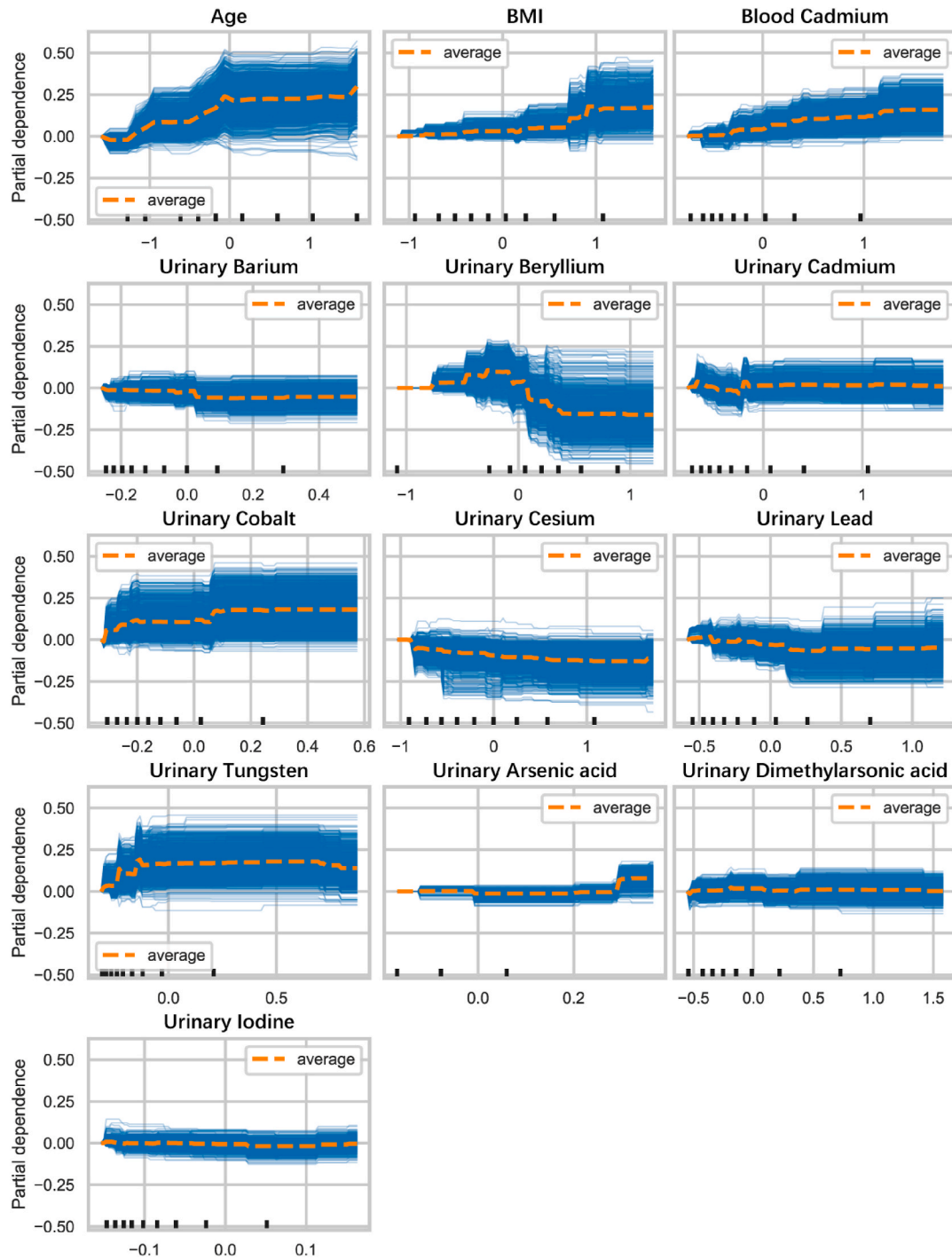


Fig. 6. Individual conditional Expectation (ICE) plots. This figure presents the ICE diagrams for each feature, enabling the examination of the effect of a single variable on predictions while eliminating the noise introduced by interactions with other features. Each thin blue line in the plot represents an individual observation, showcasing how the predicted response varies as the feature value changes, and each orange dashed line represents the average level. (For interpretation of the references to color in this figure legend, the reader is referred to the Web version of this article.)

complex interactions. Understanding these relationships not only furthers our knowledge of environmental determinants of cardiovascular disease but also emphasizes the need for continuous monitoring and potential regulatory measures regarding heavy metal exposure.

GBDT, the best prediction machine learning model in our study, is an ensemble learning technique that sequentially builds multiple decision trees, with each tree trained to correct the errors of its predecessor. The iterative approach allows GBDT to progressively minimize the residual errors through a method known as gradient descent [40,41]. GBDT

exhibits robustness against overfitting and has superior predictive accuracy compared to traditional models [41]. The capacity of GBDT to capture complex nonlinear relationships within the data is particularly pertinent in the context of researches where the relationships between features and targets are intricate, such as our study about the complex relationship between heavy metals and heart failure. In this study, we specifically focused on participants aged 50 years and older within the NHANES database. This demographic selection is particularly important given that older adults not only experience higher morbidity rates [42]

[55–57]. Additionally, there is a documented correlation between age and the duration of heavy metal exposure [58], and excessive accumulation of heavy metals in the human body may increase the risk of PhenoAge acceleration [59].

The value of our research lies in its multifaceted approach, leveraging advanced computational techniques to enhance the understanding of environmental risk factors associated with heart failure. By integrating machine learning, we move beyond traditional statistical methods, enabling the identification of complex, nonlinear relationships. Furthermore, the significance of our findings contributes to the growing evidence linking heavy metals to adverse cardiovascular outcomes, highlighting potentially modifiable risk factors for clinical practice and public health strategies.

5. Limitation

While our study offers valuable insights into the relationship between heavy metal exposure and heart failure, several limitations warrant consideration. First, despite the GBDT model achieving an accuracy of 0.78, a high sensitivity of 0.93, and a strong AUC of 0.92, the model's relatively low precision and FDR indicate a need for refinement in its predictive capabilities. This suggests that the model may generate a considerable number of false positives, which can impact clinical decision-making. Second, while the use of machine learning algorithms has improved predictive accuracy compared to traditional methods, their inherent complexity may limit interpretability, which could impede acceptance in practical applications. Third, the cross-sectional design of the study restricts our ability to infer causality. While the observed associations are significant, they do not establish a direct cause-and-effect relationship between heavy metal exposure and heart failure outcomes.

6. Conclusion

In this study, GBDT demonstrated superior performance in modeling the relationship between heavy metal exposure and heart failure. Our analysis revealed that elevated concentrations of urinary iodine, blood cadmium, urinary cobalt, urinary tungsten, and urinary arsenic acid were significantly positively associated with heart failure, while urinary beryllium appears to have a potentially detrimental effect. Additionally, we uncovered a synergistic relationship involving both age and BMI that amplifies the adverse effects of heavy metal exposure on heart failure. These findings highlight the critical need for further research to explore the underlying mechanisms and to guide targeted interventions addressing heavy metal exposure in vulnerable populations.

CRedit authorship contribution statement

Yang Yuting: Writing – review & editing, Writing – original draft, Visualization, Validation, Supervision, Software, Resources, Project administration, Methodology, Investigation, Formal analysis, Data curation, Conceptualization. **Deng Shan:** Writing – review & editing, Writing – original draft, Visualization, Validation, Supervision, Software, Resources, Project administration, Methodology, Investigation, Formal analysis, Data curation.

Data availability

The datasets generated and analyzed during the current study are available in the NHANES repository, which can be accessed at <https://www.cdc.gov/Nchs/Nhanes>.

Appendix A. Supplementary data

Supplementary data to this article can be found online at <https://doi.org/10.1016/j.ijcrp.2025.200418>.

References

- [1] L. Järup, Hazards of heavy metal contamination, *Br. Med. Bull.* 68 (2003) 167–182.
- [2] G.A. Lamas, et al., Contaminant metals as cardiovascular risk factors: a scientific statement from the American heart association, *J. Am. Heart Assoc.* 12 (2023) e029852, <https://doi.org/10.1161/JAHA.123.029852>.
- [3] L. Lind, et al., Key characteristics of cardiovascular toxicants, *Environ. Health Perspect.* 129 (2021) 95001, <https://doi.org/10.1289/EHP9321>.
- [4] P. Singh, T.E. O'Toole, D.J. Conklin, B.G. Hill, P. Haberzettl, Endothelial progenitor cells as critical mediators of environmental air pollution-induced cardiovascular toxicity, *Am. J. Physiol. Heart Circ. Physiol.* 320 (2021) H1440–H1455, <https://doi.org/10.1152/ajpheart.00804.2020>.
- [5] Z. Pan, T. Gong, P. Liang, Heavy metal exposure and cardiovascular disease, *Circ. Res.* 134 (2024) 1160–1178, <https://doi.org/10.1161/CIRCRESAHA.123.323617>.
- [6] Q. Jiang, et al., Associations of plasma metal concentrations with incident dyslipidemia: prospective findings from the Dongfeng-Tongji cohort, *Chemosphere* 285 (2021) 131497, <https://doi.org/10.1016/j.chemosphere.2021.131497>.
- [7] M. Marques, et al., Alteration of the soluble guanylate cyclase system in the vascular wall of lead-induced hypertension in rats, *J. Am. Soc. Nephrol.* 12 (2001) 2594–2600, <https://doi.org/10.1681/ASN.V12122594>.
- [8] Z. Fu, S. Xi, The effects of heavy metals on human metabolism, *Toxicol. Mech. Methods* 30 (2020) 167–176, <https://doi.org/10.1080/15376516.2019.1701594>.
- [9] Y. Zhang, et al., Exposure to multiple heavy metals associate with aberrant immune homeostasis and inflammatory activation in preschool children, *Chemosphere* 257 (2020) 127257, <https://doi.org/10.1016/j.chemosphere.2020.127257>.
- [10] K. Zheng, et al., Epidemiological evidence for the effect of environmental heavy metal exposure on the immune system in children, *Sci. Total Environ.* 868 (2023) 161691, <https://doi.org/10.1016/j.scitotenv.2023.161691>.
- [11] A.L. Riffio-Campos, et al., In silico epigenetics of metal exposure and subclinical atherosclerosis in middle aged men: pilot results from the Aragon Workers Health Study, *Philos. Trans. R. Soc. Lond. B Biol. Sci.* 373 (2018), <https://doi.org/10.1098/rstb.2017.0084>.
- [12] C. Wang, et al., Maternal exposure to heavy metals and risk for severe congenital heart defects in offspring, *Environ. Res.* 212 (2022) 113432, <https://doi.org/10.1016/j.envres.2022.113432>.
- [13] J. Sun, et al., Relationship between maternal exposure to heavy metal titanium and offspring congenital heart defects in Lanzhou, China: a nested case-control study, *Front. Public Health* 10 (2022) 946439, <https://doi.org/10.3389/fpubh.2022.946439>.
- [14] Y. Fu, et al., Relationship between cumulative exposure to metal mixtures and heart rate among Chinese preschoolers, *Chemosphere* 300 (2022) 134548, <https://doi.org/10.1016/j.chemosphere.2022.134548>.
- [15] X. Wang, X. Han, S. Guo, Y. Ma, Y. Zhang, Associations between patterns of blood heavy metal exposure and health outcomes: insights from NHANES 2011–2016, *BMC Public Health* 24 (2024) 558, <https://doi.org/10.1186/s12889-024-17754-0>.
- [16] Q. Liu, et al., Early-life exposure to lead changes cardiac development and compromises long-term cardiac function, *Sci. Total Environ.* 904 (2023) 166667, <https://doi.org/10.1016/j.scitotenv.2023.166667>.
- [17] C.G. Sears, et al., Urinary cadmium and incident heart failure: a case-cohort analysis among never-smokers in Denmark, *Epidemiology* 33 (2022) 185–192, <https://doi.org/10.1097/EDE.0000000000001446>.
- [18] D. Tomasoni, M. Adamo, C.M. Lombardi, M. Metra, Highlights in heart failure, *ESC Heart Fail* 6 (2019) 1105–1127, <https://doi.org/10.1002/ehf2.12555>.
- [19] G. Savarese, et al., Global burden of heart failure: a comprehensive and updated review of epidemiology, *Cardiovasc. Res.* 118 (2023) 3272–3287, <https://doi.org/10.1093/cvr/cvac013>.
- [20] B. Bozkurt, et al., Heart failure epidemiology and outcomes statistics: a report of the heart failure society of America, *J. Card. Fail.* 29 (2023) 1412–1451, <https://doi.org/10.1016/j.cardfail.2023.07.006>.
- [21] J.L. Peters, T.S. Perlstein, M.J. Perry, E. McNeely, J. Weuve, Cadmium exposure in association with history of stroke and heart failure, *Environ. Res.* 110 (2010) 199–206, <https://doi.org/10.1016/j.envres.2009.12.004>.
- [22] M. Tellez-Plaza, M.R. Jones, A. Dominguez-Lucas, E. Guallar, A. Navas-Acien, Cadmium exposure and clinical cardiovascular disease: a systematic review, *Curr. Atheroscler. Rep.* 15 (2013) 356, <https://doi.org/10.1007/s11883-013-0356-2>.
- [23] M. Tellez-Plaza, et al., Cadmium exposure and incident cardiovascular disease, *Epidemiology* 24 (2013) 421–429, <https://doi.org/10.1097/EDE.0b013e31828b0631>.
- [24] K.E. Deering, et al., Low-level cadmium exposure and cardiovascular outcomes in elderly Australian women: a cohort study, *Int. J. Hyg Environ. Health* 221 (2018) 347–354, <https://doi.org/10.1016/j.ijheh.2017.12.007>.
- [25] J. Guo, L. Su, X. Zhao, Z. Xu, G. Chen, Relationships between urinary antimony levels and both mortalities and prevalence of cancers and heart diseases in general US population, *NHANES 1999–2010*, *Sci. Total Environ.* 571 (2016) 452–460, <https://doi.org/10.1016/j.scitotenv.2016.07.011>.
- [26] M. Packer, Cobalt cardiomyopathy: a critical reappraisal in light of a recent resurgence, *Circ Heart Fail* 9 (2016).
- [27] X. Li, et al., Development of an interpretable machine learning model associated with heavy metals' exposure to identify coronary heart disease among US adults via SHAP: findings of the US NHANES from 2003 to 2018, *Chemosphere* 311 (2023) 137039, <https://doi.org/10.1016/j.chemosphere.2022.137039>.
- [28] G.S. Handelman, et al., eDoctor: machine learning and the future of medicine, *J. Intern. Med.* 284 (2018) 603–619, <https://doi.org/10.1111/joim.12822>.
- [29] Vallabhaneni, R., Dontu, S. & Pareek, P. K. Method for Interpreting Predictions of Black-Box Machine Learning Models, Involves Performing Interpretation of

- Explanations as Feature Importance Plots or Individual Instance Explanations by Utilizing Interactive Visualizations. IN202441008787-A.
- [30] G. Van den Broeck, A. Lykov, M. Schleich, D. Suciu, On the tractability of SHAP explanations, *J. Artif. Intell. Res.* 74 (2022) 851–886.
 - [31] C. Mou, J. Ren, Automated ICD-10 code assignment of nonstandard diagnoses via a two-stage framework, *Artif. Intell. Med.* 108 (2020) 101939, <https://doi.org/10.1016/j.artmed.2020.101939>.
 - [32] D.J. Stekhoven, P. Bühlmann, MissForest—non-parametric missing value imputation for mixed-type data, *Bioinformatics* 28 (2012) 112–118, <https://doi.org/10.1093/bioinformatics/btr597>.
 - [33] J.Y.L. Chan, et al., Mitigating the multicollinearity problem and its machine learning approach: a review, *Mathematics* 10 (2022), <https://doi.org/10.3390/math10081283>.
 - [34] E.A.P.A. Gustavo, R.C.P. Batista, Maria Carolina Monard, A study of the behavior of several methods for balancing machine learning training data, *SIGKDD Explor. Newsl* 6 (2004) 20–29, <https://doi.org/10.1145/1007730.1007735>.
 - [35] T.C.C. Lui, D.D. Gregory, M. Anderson, W.-S. Lee, S.A. Cowling, Applying machine learning methods to predict geology using soil sample geochemistry, *Appl. Comput. Geosci.* 16 (2022) 100094, <https://doi.org/10.1016/j.acags.2022.100094>.
 - [36] M.H. Saeed, J.I. Hama, Cardiac disease prediction using AI algorithms with SelectKBest, *Med. Biol. Eng. Comput.* 61 (2023) 3397–3408, <https://doi.org/10.1007/s11517-023-02918-8>.
 - [37] E. Schaffernicht, R. Kaltenhaeuser, S.S. Verma, H.M. Gross, ARTIFICIAL NEURAL NETWORKS-ICANN 2010, PT I, 6352, 2010, 362–+.
 - [38] J. Wainer, G. Cawley, Nested cross-validation when selecting classifiers is overzealous for most practical applications, *Expert Syst. Appl.* 182 (2021), <https://doi.org/10.1016/j.eswa.2021.115222>.
 - [39] A. Vij, P. Nanjundan, MOBILE COMPUTING AND SUSTAINABLE INFORMATICS, 68, 2022, pp. 585–592.
 - [40] J.H. Friedman, Stochastic gradient boosting, *Comput. Stat. Data Anal.* 38 (2002) 367–378, [https://doi.org/10.1016/S0167-9473\(01\)00065-2](https://doi.org/10.1016/S0167-9473(01)00065-2).
 - [41] C. Zhang, C. Liu, X. Zhang, G. Alpanidis, An up-to-date comparison of state-of-the-art classification algorithms, *Expert Syst. Appl.* 82 (2017) 128–150, <https://doi.org/10.1016/j.eswa.2017.04.003>.
 - [42] H. Wang, et al., Prevalence and incidence of heart failure among urban patients in China: a national population-based analysis, *Circ Heart Fail* 14 (2021) e008406, <https://doi.org/10.1161/CIRCHEARTFAILURE.121.008406>.
 - [43] A. Elbadawi, et al., Age-specific trends and outcomes of hospitalizations with acute heart failure in the United States, *Int. J. Cardiol.* 330 (2021), <https://doi.org/10.1016/j.ijcard.2021.02.031>.
 - [44] B. Fagerberg, L. Barregard, Review of cadmium exposure and smoking-independent effects on atherosclerotic cardiovascular disease in the general population, *J. Intern. Med.* 290 (2021) 1153–1179, <https://doi.org/10.1111/joim.13350>.
 - [45] J. Kim, et al., Smoking and passive smoking increases mortality through mediation effect of cadmium exposure in the United States, *Sci. Rep.* 13 (2023) 3878, <https://doi.org/10.1038/s41598-023-30988-z>.
 - [46] X. Xing, et al., Association of selenium and cadmium with heart failure and mortality based on the National Health and Nutrition Examination Survey, *J. Hum. Nutr. Diet.* 36 (2023) 1496–1506, <https://doi.org/10.1111/jhn.13107>.
 - [47] D.M. Hollins, et al., Beryllium and lung cancer: a weight of evidence evaluation of the toxicological and epidemiological literature, *Crit. Rev. Toxicol.* 39 (Suppl 1) (2009), <https://doi.org/10.1080/10408440902837967>.
 - [48] J.K. Wagoner, P.F. Infante, D.L. Bayliss, Beryllium: an etiologic agent in the induction of lung cancer, nonneoplastic respiratory disease, and heart disease among industrially exposed workers, *Environ. Res.* 21 (1980) 15–34.
 - [49] E. Ward, A. Okun, A. Ruder, M. Fingerhut, K. Steenland, A mortality study of workers at seven beryllium processing plants, *Am. J. Ind. Med.* 22 (1992) 885–904.
 - [50] A.C. Cheung, et al., Systemic cobalt toxicity from total hip arthroplasties: review of a rare condition Part 1 - history, mechanism, measurements, and pathophysiology, *Bone Joint Lett. J* 98-B (2016), <https://doi.org/10.1302/0301-620X.98B1.36374>.
 - [51] C.C. Wyles, et al., Myocardial cobalt levels are elevated in the setting of total hip arthroplasty, *J. Bone Joint Surg Am* 99 (2017) e118, <https://doi.org/10.2106/JBJS.17.00159>.
 - [52] A.E. Nigra, et al., Urinary tungsten and incident cardiovascular disease in the Strong Heart Study: an interaction with urinary molybdenum, *Environ. Res.* 166 (2018) 444–451, <https://doi.org/10.1016/j.envres.2018.06.015>.
 - [53] I. Shiu, Urinary environmental chemical concentrations and vitamin D are associated with vision, hearing, and balance disorders in the elderly, *Environ. Int.* 53 (2013) 41–46, <https://doi.org/10.1016/j.envint.2012.12.006>.
 - [54] A.A. Oyagbemi, et al., Kolaviron attenuated arsenic acid induced-cardiorenal dysfunction via regulation of ROS, C-reactive proteins (CRP), cardiac troponin I (CTnI) and BCL2, *J. Tradit. Complement. Med.* 8 (2018) 396–409, <https://doi.org/10.1016/j.jtcme.2017.05.003>.
 - [55] Y.-J. Yu, et al., Why do people gain belly fat in rural areas? A study of urinary metal (loid)s and abdominal obesity in China, *Environ. Sci. Technol.* 57 (2023) 7938–7949, <https://doi.org/10.1021/acs.est.2c09464>.
 - [56] T. Shen, et al., Associations between metal(loid) exposure with overweight and obesity and abdominal obesity in the general population: a cross-sectional study in China, *Chemosphere* 350 (2024) 140963, <https://doi.org/10.1016/j.chemosphere.2023.140963>.
 - [57] X. Wang, B. Mukherjee, S.K. Park, Associations of cumulative exposure to heavy metal mixtures with obesity and its comorbidities among U.S. adults in NHANES 2003–2014, *Environ. Int.* 121 (2018) 683–694, <https://doi.org/10.1016/j.envint.2018.09.035>.
 - [58] M. Wang, et al., Long-term heavy metal pollution and mortality in a Chinese population: an ecologic study, *Biol. Trace Elem. Res.* 142 (2011) 362–379, <https://doi.org/10.1007/s12011-010-8802-2>.
 - [59] Y. Liu, Z. Jin, S. Fu, Threshold and combined effects of heavy metals on the risk of phenotypic age acceleration among U.S. adults, *Biometals* (2024), <https://doi.org/10.1007/s10534-024-00609-x>.